Opt Quant Electron (2016) 48:206
DOI 10.1007/s11082-015-0323-y

All fiber Fabry–Pérot interferometer for high-sensitive micro-displacement sensing

Yan Bai[1] · Fengping Yan[1] · Shuo Liu[1] · Xiaodong Wen[1]

Received: 29 July 2015 / Accepted: 12 November 2015 / Published online: 23 February 2016

Abstract A fiber-optic displacement sensor based on Fabry–Pérot interferometer (FPI) with high sensitivity is investigated in both numerical simulation and experiment. The end faces of two fiber tips are applied as the mirrors to compose the Fabry–Pérot cavity (FPC). The variable lengths of the FPC will introduce different fringe spacings (FS) of the FPI transmission spectrum. With respect to this characteristic, the micro-displacement can be sensed by the FS of the transmission spectrum. Maximum sensitivity of 56.6 nm/μm, which is much higher than the previous fiber sensors, has been achieved experimentally. Due to the advantages of extremely simple configuration and manufacturing operation, the sensor is significantly beneficial to practical application.

Keywords Fiber-optic sensor · Displacement sensor · Fabry–Pérot interferometer

1 Introduction

Fiber-optic sensors have been widely demonstrated and applied for several decades attribute to their advantages of high accuracy, light weight, low cost, compact configuration, resistance to corrosion and anti-electromagnetic interference. They can be used to detect almost any parameters, such as refractive index, strain, temperature, acceleration, angle, bending radian, displacement/distance, humidity, liquid level and so on. Among them, high precision displacement fiber sensors play the most important roles in modern processing industry. Several fiber-optic methods have been applied to displacement measurement, mainly including intensity-based sensors and interferometric sensors. Intensity-based sensors (Kuang et al. 2010; Shan et al. 2014; Tang et al. 2014) are almost the first types of

✉ Fengping Yan
fpyan@bjtu.edu.cn

[1] Key Laboratory of All Optical Network and Advanced Telecommunication Network of EMC, Beijing Jiaotong University, Beijing 100044, China

fiber displacement measurement systems which have been used for commercial purpose for more than 40 years. These types of sensors, which consist of the optical sources and detectors, commonly transmit the light from the source to the object and then to the detector via fibers. Although such sensors have the advantages of simple configuration and low price, they suffer from the disadvantages of low sensitivity and poor stability. Comparatively, the interferometric sensors are more stable and sensitive than the intensity-based sensors, especially for displacement and distance detecting. Many kinds of fiber interferometers have been reported in the literatures, such as Mach–Zehnder interferometer (Wen et al. 2014; Xu et al. 2014), Michelson interferometer (MI) (Rong et al. 2013; Cheymol et al. 2014), Sagnac interferometer (SI) (Bravo et al. 2012), and Fabry–Pérot interferometer (FPI) (Li et al. 2015; Xiong et al. 2014). Specifically, the in-line Mach–Zehnder interferometer (MZI) is a common structure whose optical splitter and combiner are acted by two separated components. However, the two components are difficult to be fabricated with the concordant structure parameter, which will lead to unforeseeable transmission spectrum. On the other hand, due to the influence of two separated arms, the MZI which is composed of two cascaded fiber couplers is instable when it comes to external temperature fluctuation or mechanical vibration. MI, whose configuration is similar to MZI, has to confront with the same challenge as MZI. In contrast, SI and FPI share the same component for splitting and combining the light. Moreover, both paths of light transmit in the same fiber, which presents strong capacity of resisting disturbance. Expensive polarization maintaining fibers are necessary for most SI structures, so they always bring high cost. What's more is that the sensitivities of the previous displacement sensors mentioned above are not high enough. However, the FPI can gain higher sensitivity with simple structures and low cost, both from the performance and economic aspects. Up to now, the fiber FPIs have been applied in many sensing fields, such as temperature (Wu et al. 2015a), refractive index (Zhang and Peng 2015), pressure (Zhu et al. 2015) and displacement (Jauregui-Vazquez et al. 2013). However, the FPIs mentioned above still have the potential to simplify their designs and improve the sensitivities.

In this paper, an all fiber FPI is investigated and applied to micro-displacement sensing. The Fabry–Pérot cavity (FPC) is composed of the end faces of two fibers whose reflectivity are the main factors to affect the curve shape of the FPI transmission spectrum, which can be learned via the numerical simulation in section II. Meanwhile, the characteristic that the fringe spacing (FS) of the transmission spectrum is related to the cavity length of the FPI is applied to sensing the displacement. Besides, the experimental result shows that maximum sensitivity is as high as 56.6 nm/μm which is much higher than the reported fiber sensors (Chen et al. 2014; Meng et al. 2015; Wu et al. 2015b; Wen et al. 2014; Qi et al. 2013). In addition, the FPI possesses the advantage of simple structure and low cost, which is beneficial to engineering application.

2 Design and numerical simulation

The proposed all fiber FPI, which consists of two fiber end faces, is applied to detecting micro-displacement as shown in Fig. 1. The end faces of two fibers can be deemed as the semi-reflective mirrors whose reflectivity are determined by the coating films on the end faces.

The transmission spectrum intensity of the FPI can be given as (Zhong et al. 2012)

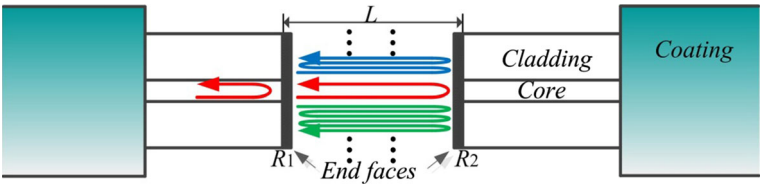

Fig. 1 Schematic diagram of the FPI for displacement sensing. The *arrows* indicate the transmission paths of light

$$I(\lambda) = I_1(\lambda) + I_2(\lambda) + 2\sqrt{I_1(\lambda)I_2(\lambda)}\cos(\Delta\varphi), \tag{1}$$

where I_1 and I_2 are two paths of light reflected by the fiber end faces, λ is the wavelength in vacuum. $\Delta\varphi$ is the optical phase difference between two paths of light, and it can be obtained

$$\Delta\varphi = \frac{2\pi}{\lambda} \cdot 2L, \tag{2}$$

where L is the length of the FPC, and the intensities of both paths of light can be expressed as

$$\begin{aligned} I_1 &= R_1 \cdot I_{in} \\ I_2 &= (1 - R_1)^2 R_2 \cdot I_{in} \end{aligned} \tag{3}$$

where R_1 and R_2 are the reflectivity of end faces of the left fiber and the right fiber respectively as shown in Fig. 1. I_{in} is the intensity of the input light. All these parameters are defined in Table 1, which are only used for numerical simulation.

In order to investigate the influence of reflectivity of the fiber end faces on transmission spectra, the path of light, which is reflected by the right fiber end for only once, is considered as the single path that can interfere with the light reflected by the left fiber end. Both paths of light are marked with red arrows in Fig. 1. The extinction ratios (ER) and maximum intensities of transmission spectra with various R_1 and R_2 are shown in Fig. 2. It can be seen that maximum ER arises when the condition of $R_1 < 40$ % is satisfied; higher-intensity (lower transmission loss) can be achieved with a larger R_2. Thus, smaller R_1 and larger R_2 should be satisfied simultaneously so that higher ER and lower transmission loss of the proposed FPI can be achieved. In fact, under the condition that only two paths of light are considered, maximum ER and minimum transmission loss can be obtained when $R_1 = 39$ % and $R_2 = 100$ %. However, larger R_1 and R_2 can introduce multiple reflections

Table 1 Parameters in the numerical simulation

Symbol	Quantity	Values
I_{in}	Intensity of the input	1 mW
R_1	Reflectivities of end faces of the left fiber	1–100 %
R_2	Reflectivities of end faces of the right fiber	1–100 %
λ	Wavelength in vacuum	1200–1900 nm
L	Length of the FPC	4–20 μm

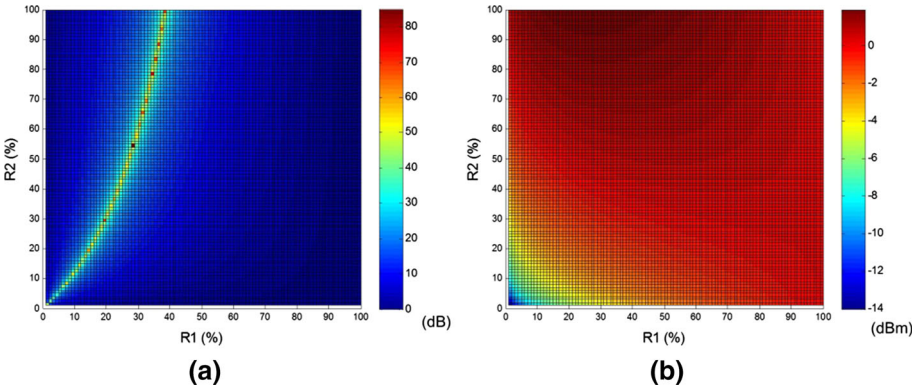

Fig. 2 The transmission spectrum with various R_1 and R_2. **a** Extinction ratio, **b** transmission intensity

which will deteriorate the transmission spectrum. Therefore, multiple reflections are taken into account in the following analysis.

The signal can be reflected back and forth between the two fiber end faces, and the more times of reflections, the lower the light intensity will be. However, the transmission spectrum can be influenced obviously by the multiple reflections of the two fiber ends when their reflectivities are high enough. All paths of light, whose intensities could not be ignored, will interfere with each other. As a result, Eq. (1) can be rewritten as

$$I = \sum_{i=1}^{M} I_i(\lambda) + \sum_{i=1}^{M} \sum_{j=1, j\neq i}^{M} \sqrt{I_i(\lambda) I_j(\lambda)} \cos\left(\Delta\varphi_{ij}\right), (M = 2, 3, 4, \ldots), \tag{4}$$

where M is the number of light paths which are taken into account in the numerical simulation. Similarly, the OPD and intensities of the light have the following forms

$$\begin{aligned} \Delta\varphi_{mn} &= \frac{2\pi}{\lambda} \cdot 2|m-n|L, (m \neq n) \\ I_1(\lambda) &= R_1 \cdot I_{in}(\lambda) \\ I_n(\lambda) &= (1-R_1)^2 (R_1 R_2)^{n-2} R_2 \cdot I_{in}(\lambda), (n = 2, 3, 4) \end{aligned} \tag{5}$$

Illustrated by the example of $R_1 = 39$ % and $R_2 = 100$ %, different values of M will lead to different transmission spectra. The value of M is infinite when the loss of light is ignored, which will increase the difficulty of the theoretical calculation; thus, $M = 2, 3, \ldots$ and 10 are taken into account as shown in Fig. 3. It can be seen that the curve gets far away from sinusoid with the increase of M; meanwhile, the average intensity (I_{ave}) of the transmission spectrum is rather more approximate to the input intensity (I_{in}). In addition, the distinction between two spectra with larger M is not as enormous as the one with smaller M. In other words, the curves with $M = 2$ and $M = 3$ are quite different from each other, but the ones with $M = 8$, 9 and 10 are almost the same. In terms of the average intensity of the transmission spectrum, the intensities of the multiple reflected paths of light are so low that their contribution to the transmission spectrum can be neglected in the numerical simulation.

Besides, the reflectivities of both fiber ends can also influence the curve shape of the transmission spectrum. Here, we assume that all the light can be received from the left

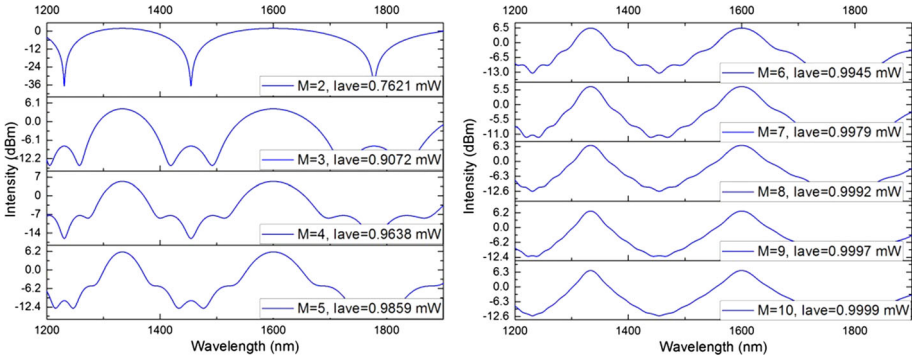

Fig. 3 The transmission spectra of the FPI with various values of M when R1 = 39 %, R2 = 100 % and L = 4 μm

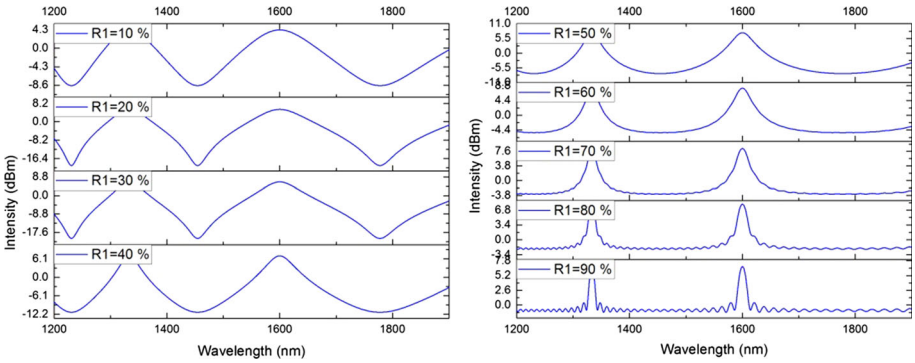

Fig. 4 The transmission spectra of the proposed FPI with various values of R_1 when $M = 20$, $R_2 = 100$ % and $L = 4$ μm

fiber, and R_2 should be set as 100 % correspondingly. With different values of R_1, various curves can be achieved as shown in Fig. 4. The bandwidths of the peaks decrease with the increase of R_1, and the curve shape is far away from sinusoid due to the overlap of multiple paths of light. As a displacement sensor, the proposed FPI can establish the relationship between transmission spectrum and the corresponding displacement generated by various cavity lengths (L) of the FPI. As is well known, there are several parameters of the transmission spectrum can be used for sensing the displacement, such as intensity, wavelength, and so on. In this article, the value of FS is applied to sensing the cavity length of the FPI. Therefore, the FS of the transmission spectrum, which is a important parameter for this kind of sensor, can be expressed as (Tian et al. 2008),

$$FS(L,\lambda) = \frac{\lambda^2}{2mL}, \quad (m = 1, 2, 3, \ldots), \tag{6}$$

where m is defined as the order difference of two optical paths (The first order of path is defined as light path reflected by the left fiber end face only once, i.e., the first order one is not reflected by the right fiber end face. The second order one and the third one are

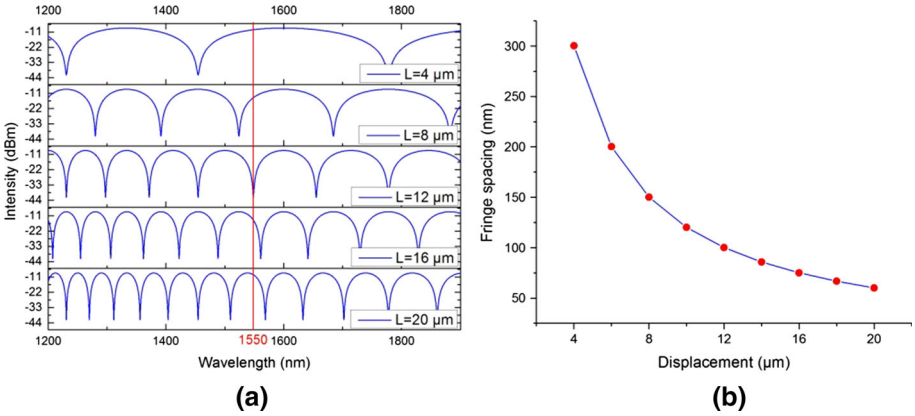

Fig. 5 **a** The transmission spectra of the FPI variation of L; **b** the FS as the function of the displacement

reflected by the right fiber end face for once and twice, respectively, and the rest can be done in the same manner). The FS will get smaller when m is becoming larger. However, it can be deduced by comparing the curves in Fig. 3 that higher order reflected paths of light are less effective to the FS.

Even when the reflectivity are as high as $R_1 = 90$ % and $R_2 = 100$ %, the high order reflected light is still irrelevant to the FS between two adjacent main peaks. In order to simplify the calculation, we assume that the first two orders of paths are taken into account when R_1 and R_2 are smaller, which is approximately consistent with the simulation result in Fig. 4. From Eq. (6). It can be seen that the value of FS is the function of λ and L; therefore, the center wavelength should be set as a constant number (take 1550 nm for instance) for the displacement sensing system. Figure 5 shows the transmission spectra of the FPI with various L from 4 to 20 μm.

From both Eq. (6) and Fig. 5b, it can be seen that FS and displacement have the relationship of inverse proportion. As a result, the sensitivity of the proposed FPI can be derived from Eq. (6) as follows

$$\frac{dFS(L,\lambda_0)}{dL} = -\frac{\lambda_0^2}{2L^2}, \tag{7}$$

where λ_0 is the reference wavelength, and it is set as 1550 nm. The minus in the right hand, which is not relevant to the sensitivity, indicates that the FS decreases with the increase of L. Ignoring the minus, the sensitivity of the FPI can be described as shown in Fig. 6. It can be recognized that the smaller the displacement, the higher the sensitivity.

3 Experimental results and analysis

The experimental setup is illustrated in Fig. 7. A 50:50 optical coupler is used to link the broadband source (BBS, Koheras Co., SuperK), the FPI and the optical spectrum analyzer (OSA, YOKOGAWA, AQ6375). The useless light of the fiber pigtails is absorbed by the refractive index matching fluid (RIMF). According to the results of numerical simulation, sensitivity of the proposed FPI is irrelevant to the reflectivity of the fiber ends. Besides, Fresnel reflection of the fiber end faces can provide the reflectivity of 4 %, which will lead

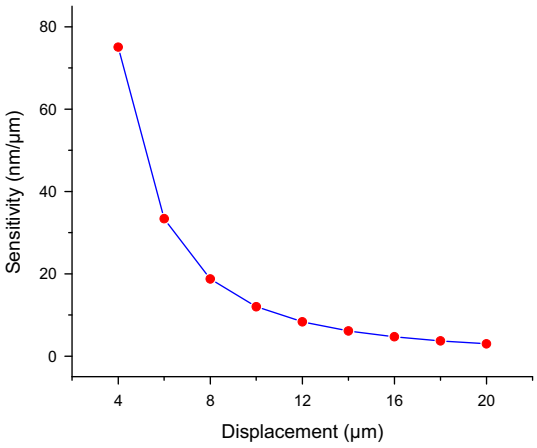

Fig. 6 The sensitivity of the FPI as the function to the displacement

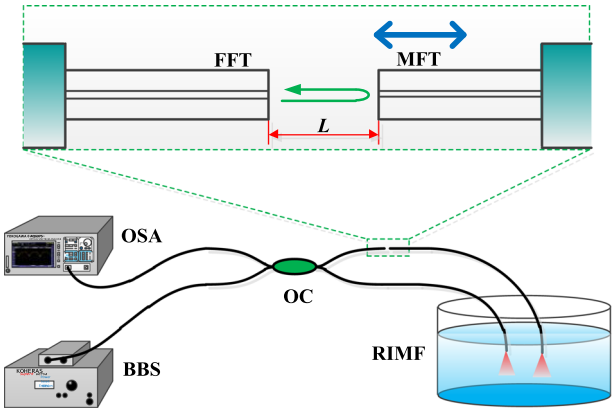

Fig. 7 Schematic diagram of the micro-displacement sensor based on all fiber FPI

to the transmission spectrum is in a state of high ER and low intensity as shown in Fig. 2. Thus, there is no additional coating film is implemented on the fiber ends. The operating wavelength of BBS and OSA are both set as 1200–1900 nm which is corresponding to the numerical simulation in section II.

Figure 8 shows the transmission spectra of the FPI with various lengths of FPC. Both FS and ER of the transmission spectrum drop down with the increase of displacement; meanwhile, the curve shapes are close to sine curves. Maximum ER of more than 15 dB is achieved when the length of FPC is about 3 μm. Fast Fourier transform algorithm is applied to analyzing the number of light paths as shown in Fig. 9 from which two obvious peaks can be seen when $L = 3$ μm is satisfied. In other words, it explains that more than three orders of paths will be involved in interference. However, the peaks intensities decline with the increase of L, thus the light intensities of optical paths with multiple reflections are much weaker than the ones with fewer times of reflections. This result agrees with the numerical simulation that low reflectivities of the fiber ends will lead to transmission spectrum closing to sine curve.

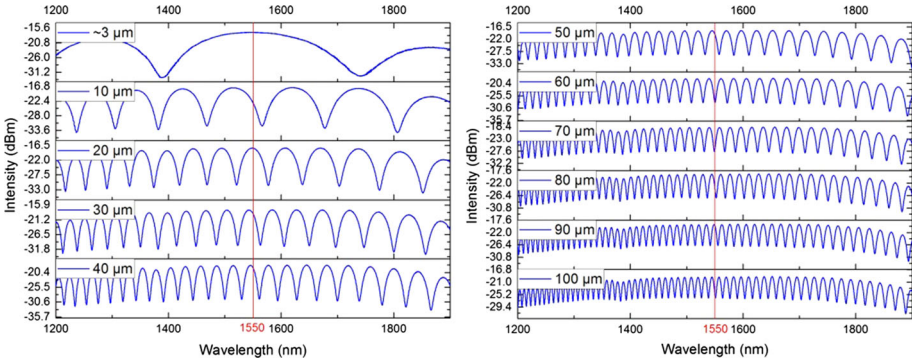

Fig. 8 The transmission spectra of the FPI with various L

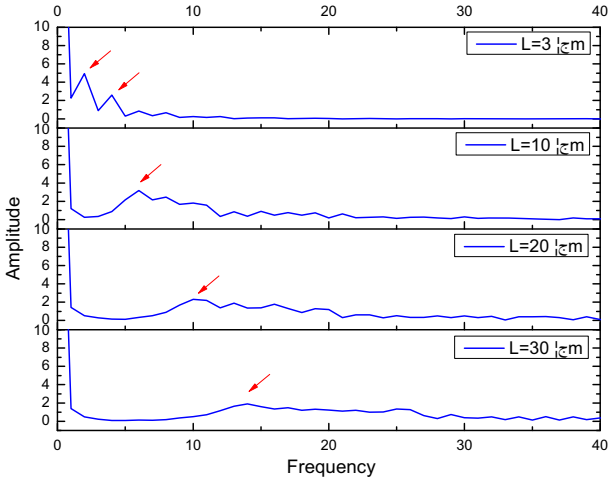

Fig. 9 Fast Fourier transform of the experimental results with FPC length of 3, 10, 20 and 30 μm

Furthermore, the relationship between the fringe spacing and displacement is shown in Fig. 10a. Meanwhile, the coefficient of determination of $R_2 = 0.9986$ is obtained after linear fitting of 1/FS, which manifests that 1/FS and displacement possess a satisfactory linear relation. In other words, fringe space of the transmission spectrum and the length of FPC have a reverse relationship, which coincides with the simulation result as shown in Fig. 5. According to the linear fitting in Fig. 10a and the expression in Eq. (7), the sensitivity of the FPI can be achieved as shown in Fig. 10b. It is proved that maximum sensitivity is approximately 56.6 nm/μm, and the sensitivity decreases with the increase of displacement. Minimum displacement of about 3 μm is implemented in our experiment; however, the sensitivity has the potential to be improved by further diminishing the length of the FPC, and the operation wavelength range of BBS and OSA should be enlarged correspondingly at this time.

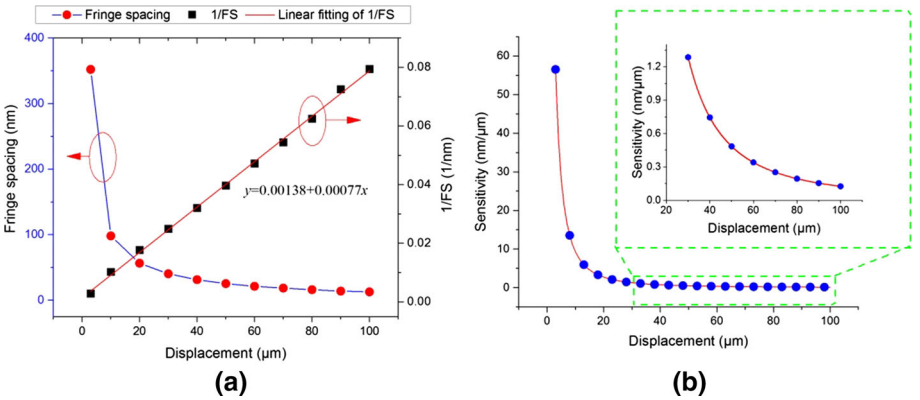

Fig. 10 **a** The FS and the 1/FS as the function to the displacement; **b** the sensitivity of the FPI as the function to the length of the FPC

4 Conclusion

In summary, we demonstrate an all fiber FPI for displacement measurement. Reflectivities of the fiber end faces can affect the bandwidths of the peaks but the FS, which can be deduced from the numerical simulation. As a result, FS of the transmission spectrum is applied to sensing length of the FPC. In addition, the experimental result shows that maximum sensitivity of 56.6 nm/μm can be achieved when the length of FPC is about 3 μm. Furthermore, the measurable displacement range, whose sensitivity is higher than 1.533 nm/μm, is 27 μm. This type of FPI has the capacity of higher sensitivity by using a smaller length of the FPC; thus it can be applied to micro-displacement sensing with super high resolution.

Acknowledgments This work is supported by the National Natural Science Foundation of China (Nos. 61275091, 61327006).

References

Bravo, M., Pinto, A.M.R., Lopez-Amo, M., Kobelke, J., Schuster, K.: High precision micro-displacement fiber sensor through a suspended-core sagnac interferometer. Opt. Lett. **37**(2), 202–204 (2012). doi:10.1364/OL.37.000202

Chen, J., Zhou, J., Yuan, X.: M–Z interferometer constructed by two S-bend fibers for displacement and force measurements. Photonics Technol. Lett. IEEE **26**(8), 837–840 (2014). doi:10.1109/LPT.2014.2308327

Cheymol, G., Gusarov, A., Gaillot, S., Destouches, C., Caron, N.: Dimensional measurements under high radiation with optical fiber sensors based on white light interferometry—report on irradiation tests. Nucl. Sci. IEEE Trans. **61**(4), 2075–2081 (2014). doi:10.1109/TNS.2014.2321026

Jauregui-Vazquez, D., Estudillo-Ayala, J.M., Castillo-Guzman, A., Rojas-Laguna, R., Selvas-Aguilar, R., Vargas-Rodriguez, E., Sierra-Hernandez, J.M., Guzman-Ramos, V., Flores-Balderas, A.: Highly sensitive curvature and displacement sensing setup based on an all fiber micro Fabry–Perot interferometer. Opt. Commun. **308**, 289–292 (2013). doi:10.1016/j.optcom.2013.07.041

Kuang, J.-H., Chen, P.-C., Chen, Y.-C.: Plastic optical fiber displacement sensor based on dual cycling bending. Sensors **10**, 10198–10210 (2010)

Li, L., Zhang, D., Wen, X., Peng, S.: FFPI-FBG hybrid sensor to measure the thermal expansion and thermo-optical coefficient of a silica-based fiber at cryogenic temperatures. Chin. Opt. Lett. **13**(10), 100601 (2015). doi:10.3788/COL201513.100601

Meng, F., Qin, Z., Rong, Q., Sun, H., Li, J., Yang, Z., Hu, M., Geng, H.: Hybrid fiber interferometer for simultaneous measurement of displacement and temperature. Chin. Opt. Lett. **13**(5), 050603 (2015). doi:10.3788/COL201513.050603

Qi, L., Zhao, C.-L., Wang, Y., Kang, J., Zhang, Z., Jin, S.: Compact micro-displacement sensor with high sensitivity based on a long-period fiber grating with an air-cavity. Opt. Express **21**(3), 3193–3200 (2013). doi:10.1364/OE.21.003193

Rong, Q., Qiao, X., Du, Y., Feng, D., Wang, R., Ma, Y., Sun, H., Hu, M., Feng, Z.: In-fiber quasi-Michelson interferometer with a core-cladding-mode fiber end-face mirror. Appl. Opt. **52**(7), 1441–1447 (2013). doi:10.1364/AO.52.001441

Shan, M., Min, R., Zhong, Z., Wang, Y., Hao, B., Zhang, Y.: Differential transmissive fiber-optic distance sensor. Microw. Opt. Technol. Lett. **56**(5), 1104–1107 (2014). doi:10.1002/mop.28275

Tang, G., Wei, J., Zhou, W., Fan, R., Wu, M., Xu, X.: Multi-hole plastic optical fiber force sensor based on femtosecond laser micromachining. Chin. Opt. Lett. **12**(9), 090604 (2014). doi:10.3788/COL201412.090604

Tian, Z., Yam, S.S.H., Barnes, J., Bock, W., Greig, P., Fraser, J.M., Loock, H.P., Oleschuk, R.D.: Refractive index sensing with Mach–Zehnder interferometer based on concatenating two single-mode fiber tapers. Photonics Technol. Lett. IEEE **20**(8), 626–628 (2008). doi:10.1109/LPT.2008.919507

Wen, X., Ning, T., You, H., Kang, Z., Li, J., Li, C., Feng, T., Yu, S., Jian, W.: Analysis and measurement of the displacement sensor based on up-tapered Mach–Zehnder interferometer. Chin. Phys. Lett. **31**(3), 034203 (2014). doi:10.1088/0256-307X/31/3/034203

Wu, D., Huang, Y., Fu, J.-Y., Wang, G.-Y.: Fiber Fabry–Perot tip sensor based on multimode photonic crystal fiber. Opt. Commun. **338**, 288–291 (2015a). doi:10.1016/j.optcom.2014.10.062

Wu, J., Miao, Y., Song, B., Lin, W., Zhang, K., Zhang, H., Liu, B., Yao, J.: Simultaneous measurement of displacement and temperature based on thin-core fiber modal interferometer. Opt. Commun. **340**, 136–140 (2015b). doi:10.1016/j.optcom.2014.11.016

Xiong, L., Zhang, D., Li, L., Guo, Y.: EFPI-FBG hybrid sensor for simultaneous measurement of high temperature and large strain. Chin. Opt. Lett. **12**(12), 120605 (2014). doi:10.388/COL201412.120605

Xu, L., Han, W., Wang, P., Wang, S.: Hybrid Mach–Zehnder interferometric sensor based on two core-of fset attenuators and an abrupt taper in single-mode fiber. Chin. Opt. Lett. **12**(7), 070602 (2014). doi:10.3788/col201412.070602

Zhang, X., Peng, W.: Temperature-independent fiber salinity sensor based on Fabry–Perot interference. Opt. Express **23**(8), 10353–10358 (2015). doi:10.1364/OE.23.010353

Zhong, C., Shen, C., You, Y., Chu, J., Zou, X., Dong, X., Jin, Y., Wang, J.: Temperature-insensitive optical fiber two-dimensional micrometric displacement sensor based on an in-line Mach–Zehnder interferometer. J. Opt. Soc. Am. B **29**(5), 1136–1140 (2012). doi:10.1364/JOSAB.29.001136

Zhu, J., Wang, M., Shen, M., Chen, L., Ni, X.: An optical fiber Fabry–Pérot pressure sensor using an SU-8 structure and angle polished fiber. Photonics Technol. Lett. IEEE **27**(19), 2087–2090 (2015). doi:10.1109/LPT.2015.2453318